

**Self-Assembly of Nanosheet Supported Fe-MOFs  
Heterocrystal as Reusable Catalyst for Boosting Advanced  
Oxidation Performance via Radical and Nonradical  
Pathways**

ZHANG, Bofan, ZHANG, Liang, AKIYAMA, Kazuhiko, BINGHAM, Paul  
<<http://orcid.org/0000-0001-6017-0798>>, ZHOU, Yingtang and KUBUKI, Shiro

Available from Sheffield Hallam University Research Archive (SHURA) at:

<https://shura.shu.ac.uk/28560/>

---

This document is the Supplemental Material

**Citation:**

ZHANG, Bofan, ZHANG, Liang, AKIYAMA, Kazuhiko, BINGHAM, Paul, ZHOU, Yingtang and KUBUKI, Shiro (2021). Self-Assembly of Nanosheet Supported Fe-MOFs Heterocrystal as Reusable Catalyst for Boosting Advanced Oxidation Performance via Radical and Nonradical Pathways. ACS Applied Materials and Interfaces. [Article]

---

**Copyright and re-use policy**

See <http://shura.shu.ac.uk/information.html>

## Supporting Information

### Self-Assembly of Nanosheet Supported Fe-MOFs Heterocrystal as Reusable Catalyst for Boosting Advanced Oxidation Performance via Radical and Nonradical Pathways

Bofan Zhang<sup>1,†,\*</sup>, Liang Zhang<sup>2,†</sup>, Kazuhiko Akiyama<sup>1</sup>, Paul A. Bingham<sup>3</sup>, Yingtang Zhou<sup>4,\*</sup>, Shiro Kubuki<sup>1</sup>

<sup>1</sup>Department of Chemistry, Tokyo Metropolitan University, Tokyo 192-0397, Japan

<sup>2</sup>Mössbauer Effect Data Center, Dalian Institute of Chemical Physics, Chinese Academy of Sciences, Dalian  
116023, China.

<sup>3</sup>College of Business, Technology and Engineering, Sheffield Hallam University, Howard Street,  
Sheffield S1 1WB, UK

<sup>4</sup>Institute of Innovation & Application, Zhejiang Ocean University, Zhoushan 316022, Zhejiang, China

\*Corresponding authors: Bofan Zhang and Yingtang Zhou

E-mail: [15054218031@163.com](mailto:15054218031@163.com) (B.F. Zhang); [376477613@qq.com](mailto:376477613@qq.com) (Y.T. Zhou)

## **S1. Chemicals**

$\text{FeCl}_3 \cdot 6\text{H}_2\text{O}$ ,  $\text{Bi}(\text{NO}_3)_3 \cdot 5\text{H}_2\text{O}$ , 1,4-benzenedicarboxylic acid (1,4-BDC), potassium iodide, N, N-dimethylformamide (DMF), polyvinylpyrrolidone (PVPK-30), absolute ethanol, p-benzoquinone, triethanolamine, and isopropyl alcohol were purchased from Siyaku Chemical Reagent Co., Ltd., Japan. All reagents used were analytical reagents.

## **S2. Synthesis of Fe-MOF catalysts**

MIL-53(Fe) was fabricated using a solvothermal method. Briefly, 5 mmol  $\text{FeCl}_3 \cdot 6\text{H}_2\text{O}$  and 5 mmol terephthalic acid were dissolved in 10 mL N, N'-dimethylformamide. After stirring for 60 min, the resultant mixture was transferred to a Teflon-lined stainless-steel container and heated at 150 °C for 3 h under autogenous pressure. After being cooled down to room temperature, the suspension was centrifuged and washed with ethanol and deionized water several times. Then 100 mL deionized water was added and the mixture was stirred for 12 h to ensure removal of DMF from pores. Finally, the material was dried at 60 °C overnight.

MIL-101(Fe) was fabricated by a solvothermal process. Briefly, 4.9 mmol of  $\text{FeCl}_3 \cdot 6\text{H}_2\text{O}$  and 2.48 mmol of  $\text{H}_2\text{BDC}$  were mixed in 30 mL of DMF and then sonicated for 15 min to ensure their dissolution. The obtained dark orange solution was transferred into a Teflon-lined stainless-steel autoclave (50 mL) and heated at 110 °C in an oven for 20 h. Finally, the resultant products were dried at 60 °C overnight.

For the synthesis of MIL-88A(Fe), 1.352 g  $\text{FeCl}_3 \cdot 6\text{H}_2\text{O}$  (5 mmol) and 0.580 g fumaric acid were dissolved in ratio of 1:1 water/DMF (N, N-dimethylformamide). The synthesized MIL-88A (Fe) was transferred into a Teflon-lined autoclave and heated at 65 °C for 4 h.

## **S3. Synthesis of BiOI/MIL-88A(Fe) and BiOI/MIL-101(Fe)**

The BiOI/MIL-53(Fe) was fabricated employing a one-step coprecipitation method. 1.02 g of  $\text{Bi}(\text{NO}_3)_3 \cdot 5\text{H}_2\text{O}$  was dissolved in 60 mL ethanol to obtain solution. Then, 0.2 g PVP was added into mixture. Afterward, an appropriate amount of MIL-53(Fe) was dissolved in the mixture and ultrasonicated for 30 min. Next, 0.3486 g KI was added and stirred for 12 h. The final precipitate was washed by water and ethanol, and dried at 60 °C. The BiOI was prepared by using same procedure except loading MIL-53(Fe). Samples synthesized with different MIL-53 (Fe)/BiOI ratio of 20, 40, 60 and 80 wt% were designated as BMFe-2, BMFe-4, BMFe-6

and BMFe-8. Detailed synthesis procedures for BiOI/MIL-88, BiOI/MIL-101, BiOCl/MIL-53 and BiOBr/MIL-53 are given in the supporting information (S2-S4).

The BiOI/MIL-88A(Fe) and BiOI/MIL-101(Fe) were prepared via a facile one-step precipitation method. Firstly, 1.02 g of  $\text{Bi}(\text{NO}_3)_3 \cdot 5\text{H}_2\text{O}$  was stirred magnetically in 60 mL of ethanol for 60 min to obtain a homogenous white suspension. Then, 0.2 g PVP was put into the mixture and stirring was resumed for 60 min. Afterward, an appropriate amount of MIL-88A(Fe) or MIL-101(Fe) was put into the mixture and ultrasonicated for 30 min. Next, 0.3486 g KI was added and the mixture was stirred for 12 h. The resulting precipitate was centrifuged and washed with deionized water and absolute ethanol, and dried at 60°C for 12 h.

#### **S4. Synthesis of BiOBr/MIL-53(Fe) and BiOCl/MIL-53(Fe)**

For the fabrication of BiOBr/MIL-53(Fe) and BiOCl/MIL-53(Fe) composites, 1.02 g of  $\text{Bi}(\text{NO}_3)_3 \cdot 5\text{H}_2\text{O}$  was stirred magnetically in 60 mL of ethanol for 60 min to obtain a homogenous white suspension. Then, 0.2 g PVP was put into the mixture and stirring was resumed for 60 min. Afterward, an appropriate amount of MIL-53(Fe) was put into the mixture and ultrasonicated for 30 min. Next, 0.2499 g KBr or 0.1570 g KCl was added and the mixture was stirred for 12 h. The resulting precipitate was centrifuged and washed with deionized water and absolute ethanol, and dried at 60°C for 12 h.

#### **S5. Characterization**

X-ray diffraction (XRD) patterns were obtained from an X-ray diffractometer with  $\text{Cu K}\alpha$  radiation, then were applied to evaluate the crystal structure of the samples. The Fourier transform-infrared (FT-IR) spectra were obtained using an FT-IR optical spectrometer (Nexus 670) in the range 500-3500  $\text{cm}^{-1}$ . The morphology and composition of BiOI were analyzed by transmission electron microscopy (TEM, JEM-3200FS) and energy-dispersive X-ray spectroscopy (EDX). Surface electronic states were recorded by X-ray photoelectron spectroscopy (XPS, VG MultiLab 2000). The  $\text{N}_2$  adsorption-desorption measurements were analyzed by the nitrogen adsorption apparatus (ASAP 2020, USA). The UV-vis diffusive reflectance spectra (DRS) of samples were analyzed on a UV-vis spectrophotometer. Photoluminescence (PL) spectra were obtained by fluorescence spectrometry (FP-6300). Electrochemical impedance spectroscopy (EIS) and Mott-Schottky were analyzed in a three-electrode system of the CHI-600E electrochemical workstation (Shanghai Chenhua, China). The total organic carbon (TOC) was analyzed using a Jena-2100 TOC analyzer.  $^{57}\text{Fe}$  Mössbauer spectra of MIL-53(Fe)

and BMFe catalysts were obtained using  $^{57}\text{Co}$  (Rh)  $\gamma$ -ray radioactive source maintained at room temperature.

EPR spectra were recorded using a Bruker ESR A300-10/12 spectrometer at room temperature.

Table S1. BET surface areas and pore diameters of BiOI, MIL-53(Fe), BMFe-4 and used BMFe-4 catalysts

Sample	BET Surface Area (m <sup>2</sup> /g)	Average pore diameter (nm)	Pore volume (cm <sup>3</sup> /g)
BiOI	10.5	1.54	0.073
MIL-53(Fe)	27.7	1.21	0.26
MBFe-4	25.8	1.75	0.17
Used MBFe-4	21.4	1.83	0.16

All samples are of type III isotherm with a hysteresis loop between the adsorption-desorption isotherms. The BET surface areas of BiOI, MIL-53 and MBFe-4 were 10.5, 27.7 and 25.8 m<sup>2</sup>/g, respectively, and the pore size were about 1.21 nm, indicating a microporous structure. While MIL-53 combining with BiOI to form heterojunction, the BET surface area was lower than before recombining with BiOI, which can be attributed to the pores of MIL-53 being blocked by the BiOI nanosheet.<sup>1</sup> Despite this, after the formation of BMFe heterojunction catalyst, the BET surface area and pore volume can still reach 25.8 m<sup>2</sup>/g and 0.17cm<sup>3</sup>/g.

Table S2. Details of the analysis of pollutants

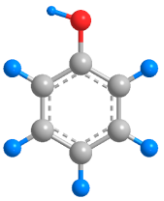
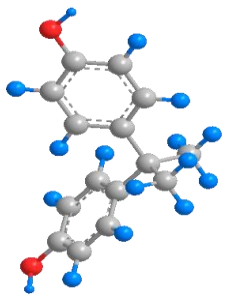
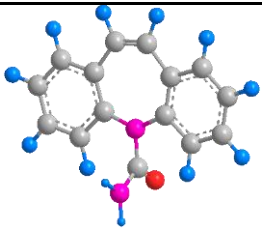
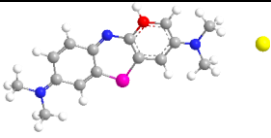
Pollutants	Method	Chemical Formula	Structure
Phenol	Measured by UV-vis and HPLC (C18 column 5 $\mu$ m, 150 mm*4.6 mm). The mobile phase consisted of Methanol and water (80:20, v/v) at a flow rate of 0.8 mL/min with the detection wavelength at 280 nm. The column temperature was held at 25 $\pm$ 0.5 $^{\circ}$ C.	C <sub>6</sub> H <sub>6</sub> O	
Bisphenol A (BPA)	Measured by HPLC (C18 column 5 $\mu$ m, 150 mm*4.6 mm). The mobile phase consisted of Methanol and water (70:30, v/v) at a flow rate of 1.0 mL/min with the detection wavelength at 230 nm. The column temperature was held at 25 $\pm$ 0.5 $^{\circ}$ C.	C <sub>15</sub> H <sub>16</sub> O <sub>2</sub>	
Carbamazepine (CBZ)	Measured by UV-vis with the detection wavelength at 285 nm. The degradation intermediates were obtained by HPLC-MS.	C <sub>15</sub> H <sub>12</sub> N <sub>2</sub> O	
Methylene Blue	Measured by UV-vis with the detection wavelength at 665 nm.	C <sub>16</sub> H <sub>18</sub> ClN <sub>3</sub> S	

Table S3. Some degradation intermediates of CBZ during photo-Fenton reaction

Products	m/z	Formula	Proposed Structure
Carbamazepine	237	C <sub>15</sub> H <sub>12</sub> N <sub>2</sub> O	
TP1	208	C <sub>15</sub> H <sub>14</sub> N	
TP2	267	C <sub>16</sub> H <sub>15</sub> N <sub>2</sub> O <sub>2</sub>	
TP3	253	C <sub>16</sub> H <sub>18</sub> N <sub>2</sub> O <sub>2</sub>	
TP4	285	C <sub>16</sub> H <sub>17</sub> N <sub>2</sub> O <sub>3</sub>	
TP5	273	C <sub>15</sub> H <sub>14</sub> NO <sub>4</sub>	
TP6	271	C <sub>16</sub> H <sub>19</sub> N <sub>2</sub> O <sub>2</sub>	
TP7	267	C <sub>16</sub> H <sub>15</sub> N <sub>2</sub> O <sub>2</sub>	
TP8	251	C <sub>15</sub> H <sub>11</sub> N <sub>2</sub> O <sub>2</sub>	
TP9	285	C <sub>16</sub> H <sub>17</sub> N <sub>2</sub> O <sub>3</sub>	
TP10	271	C <sub>15</sub> H <sub>15</sub> N <sub>2</sub> O <sub>3</sub>	
TP11	207	C <sub>14</sub> H <sub>9</sub> NO	
TP12	207	C <sub>14</sub> H <sub>9</sub> NO	
TP13	179	C <sub>13</sub> H <sub>9</sub> N	
TP14	195	C <sub>13</sub> H <sub>9</sub> NO	
TP15	197	C <sub>13</sub> H <sub>11</sub> NO	
TP16	137	C <sub>7</sub> H <sub>7</sub> NO <sub>2</sub>	
TP17	110	C <sub>6</sub> H <sub>6</sub> O <sub>2</sub>	
TP18	138	C <sub>7</sub> H <sub>6</sub> O <sub>3</sub>	



Table S4. Comparison of catalytic performance with series of previously reported catalysts for degradation of refractory organic pollutants

Catalyst	Target Pollutants	Hydrogen peroxide concentration	Light source (wavelength/nm)	Catalytic capacity		Reference
				Pseudo-first-order rate constant	Removal efficiency	
<b>Fe-g-C<sub>3</sub>N<sub>4</sub></b>	10mg/L MB	80 mM	400 W xenon lamp	0.060 s <sup>-1</sup>	99% in 60 min	Li et al. 2018 <sup>2</sup>
<b>CS/PAN@FeOOH/g-C<sub>3</sub>N<sub>4</sub></b>	50 mg/L MB	50 mM	300 W xenon lamp	0.052 min <sup>-1</sup>	99.3% in 100 min	Zheng et al. 2021 <sup>3</sup>
<b><math>\alpha</math>-Fe<sub>2</sub>O<sub>3</sub>/Bi<sub>2</sub>WO<sub>6</sub></b>	5mg/L MB	10 mM	300 W xenon lamp	0.189 min <sup>-1</sup>	98.9% in 25 min	Wang et al. 2021 <sup>4</sup>
<b>ZnFe<sub>2</sub>O<sub>4</sub>/<math>\alpha</math>-Fe<sub>2</sub>O<sub>3</sub></b>	100 mg/L MB	200 mM	300 W xenon lamp	0.059 min <sup>-1</sup>	99.96% in 100 min	Wang et al. 2020 <sup>5</sup>
<b>g-C<sub>3</sub>N<sub>4</sub>/ MIL-88B(Fe)</b>	30 mg/L MB	20 mM	500 W Xe lamp	0.0191 min <sup>-1</sup>	99.9% in 120 min	Liao et al. 2020 <sup>6</sup>
<b>BiOI/MIL-53(Fe)</b>	20 $\mu$ M MB	5 mM	100 W Hg lamp	0.292 min <sup>-1</sup>	99% in 10 min	<b>This work</b>
<b>MIL-88B-Fe/Ti<sub>3</sub>C<sub>2</sub></b>	10 mg/L Phenol	10 mM	500 W xenon lamp	--	90% in 120 min	Ahmad et al. 2020 <sup>7</sup>
<b>MIL-100(Fe)@ZnO</b>	5 mg/L Phenol	10 mM	500 W xenon lamp	--	95% in 120 min	Ahmad et al. 2019 <sup>8</sup>
<b>MIL-100(Fe)@ZnO</b>	5 mg/L Bisphenol A	10 mM	500 W xenon lamp	--	96% in 120 min	Ahmad et al. 2019 <sup>8</sup>
<b>GS-Fe-NPs</b>	25 mg/L Bisphenol A	500 mM	300 W xenon lamp	--	92% in 150 min	Guo et al. 2020 <sup>9</sup>
<b>MIL-88A(Fe)</b>	10 mg/L Bisphenol A	20 mM	300 W LED lamp	--	95% in 80 min	Fu et al. 2020 <sup>10</sup>
<b>FeOCl</b>	100 $\mu$ M Carbamazepine (CBZ)	8mM	UV light	--	90% in 30 min	Sun et al. 2020 <sup>11</sup>
<b>MIL-53(Fe)</b>	40 mg/L Carbamazepine (CBZ)	20 mM	500 W xenon lamp	--	90% in 270 min	Gao et al. 2017 <sup>12</sup>
<b>BiOI/MIL-53(Fe)</b>	20 mg/L Phenol, Bisphenol A, Carbamazepine	5 mM	100W Hg lamp	--	59% in 60 min; 90.4% in 120 min; 67% in 80 min	This work

## Supplementary Figures

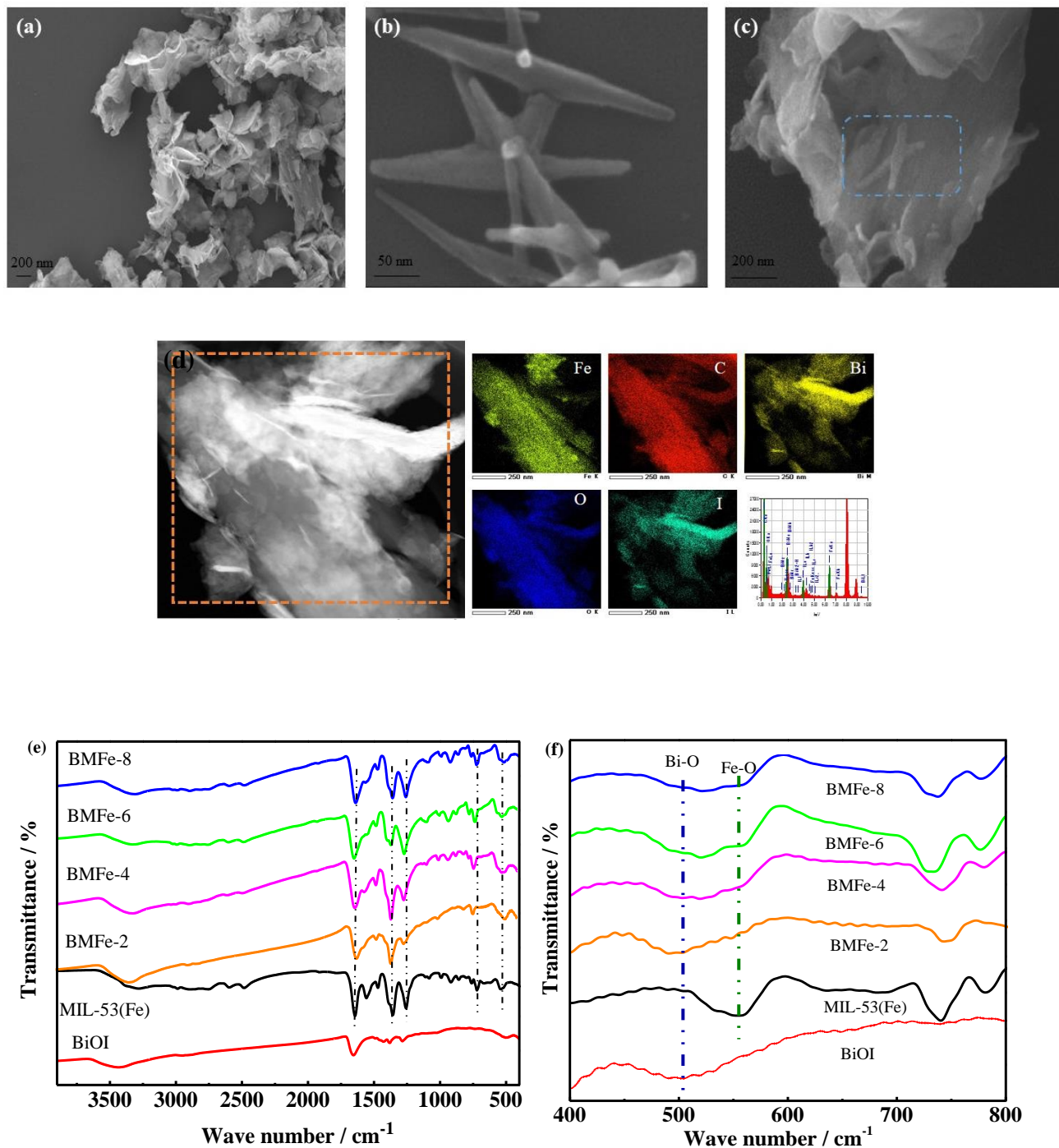


Figure S1. SEM images of BiOI (a), MIL-53(Fe) (b) and BMFe (c); Element mapping of BMFe (d); FT-IR spectra of as-prepared catalysts (e) and enlarged FT-IR spectra of as-prepared catalysts for clarity (f); The scale bar were 1  $\mu\text{m}$  (a), 50 nm (b) and 20 nm (c).

The chemical structure of BiOI and MIL-53(Fe) were investigated by FTIR spectroscopy. As shown in Figure S1e, the distinct bands of BiOI and MIL-53(Fe) could be clearly observed in spectra for BMFe composites, indicating that the structural characteristics of BiOI and MIL-53(Fe) were completely reversed after combination. This result was also consistent with the XRD pattern analysis. Moreover, the absorption peak at  $737\text{ cm}^{-1}$  is related to C-H bending vibrations of the benzene ring.<sup>13</sup> The absorption bands at  $1282$  and  $1388\text{ cm}^{-1}$  correspond to symmetrical ( $\nu_{\text{as}}(\text{C}-\text{O})$ ) and a symmetric ( $\nu_{\text{s}}(\text{C}-\text{O})$ ) vibrations of carboxyl groups.<sup>14</sup> The characteristic peak at  $1673\text{ cm}^{-1}$  is attributable to the stretching vibration of C=O bond.<sup>15</sup> These peaks are mainly derived from the terephthalic acid ligand which possesses a benzene ring and two carboxyl functional groups. The broad peak at  $3440\text{ cm}^{-1}$  corresponds to O-H stretching mode due to the water and ethanol adsorbed on the surface. The FTIR spectra with a narrower wavenumber range are depicted in Figure S1f. Evidently, the characteristic peaks at  $505\text{ cm}^{-1}$  and  $553\text{ cm}^{-1}$  are due to stretching vibrations of Bi-O bonds and Fe-O bonds in  $\text{FeO}_6$  octahedra, respectively, further revealing the successful fabrication of BMFe composites.<sup>16,17</sup>

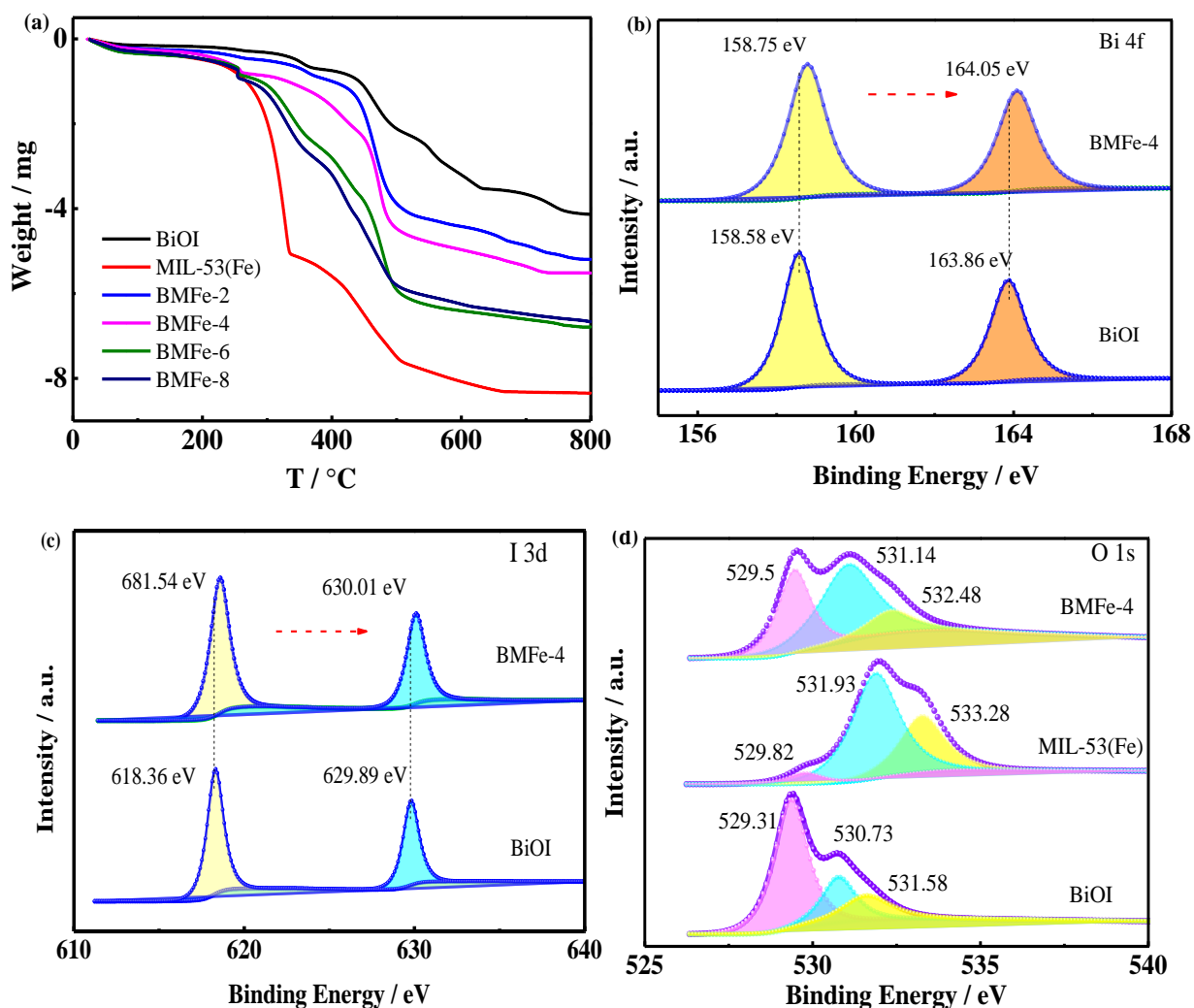


Figure S2. (a) TGA curves and XPS spectra of (b) Bi 4f, (c) I 3d, (d) O 1s in BiOI, MIL-53(Fe) and BMFe composites

The thermogravimetric analysis (TGA) curves depicted in Figure S2a were measured to analyze the thermal stability and further confirm the successful coupling between BiOI and MIL-53(Fe). The weight loss below 300 °C can be ascribed to the evaporation of guest molecules, such as free water, ethanol and bound water. At pyrolysis temperatures of 335, 504, 662 °C, various organic functional groups in MIL-53(Fe) experienced decomposition of organic structures, formation of new spatial configurations and separation of ligands.<sup>18</sup> The TGA results for all composites exhibit the decomposition characteristics of MIL-53(Fe) and BiOI, and come closer to MIL-53(Fe) as the content of MOFs increase, revealing the successful synthesis of MOFs on BiOI nanosheets. The elemental construction and surface chemical states of BiOI, MIL-53(Fe) and BMFe-4 were

revealed by X-ray photoelectron spectroscopy (XPS). As depicted in Figure S2b, the high-resolution Bi 4f spectrum could be deconvoluted into two peaks, including a component centered at 158.75 eV for Bi 4f<sub>7/2</sub>, and a component at 164.05 eV for Bi 4f<sub>5/2</sub>, respectively. For the I 3d spectrum of BiOI, the peaks could be fitted by two I components at 618.36 and 629.89 eV, which are ascribed to I 3d<sub>5/2</sub> and I 3d<sub>3/2</sub>. For the high-resolution O 1s spectrum, the peak could be deconvoluted into several O species. The characteristic peaks at 529.31, 530.73 and 531.58 eV of BiOI correspond to lattice O species, oxygen vacancy and C=O groups, respectively. The spectra peaks located at 529.82, 531.73 and 533.28 eV for MIL-53(Fe) are assigned to lattice O species, C=O groups and C-O bond in carboxylic group. After combining with BiOI and MIL-53(Fe), all of these O species were kept in the composites. This XPS result clearly revealed the surface chemical state and composition in BMFe, which is consistent with the EDS analysis.

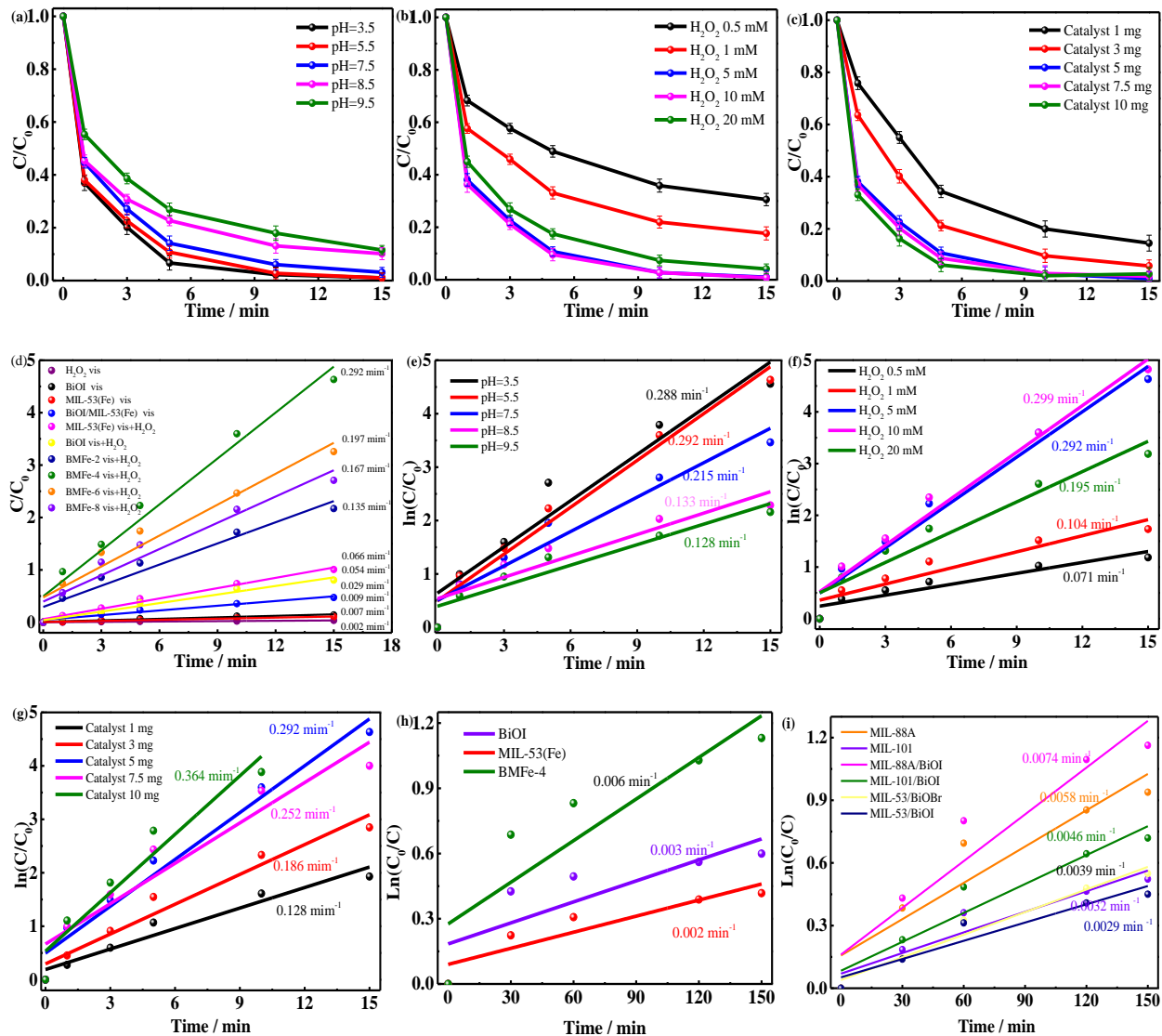


Figure S3. (a-c) Different influencing factors of the B<sub>M</sub>Fe-4 catalyst for the degradation of MB; (d-g) Pseudo-first-order kinetics of degradation of MB in different influencing factors of the B<sub>M</sub>Fe-4 catalyst; (h-i) degradation of phenol under different photo-Fenton system (Fe-MOFs/BiOX)

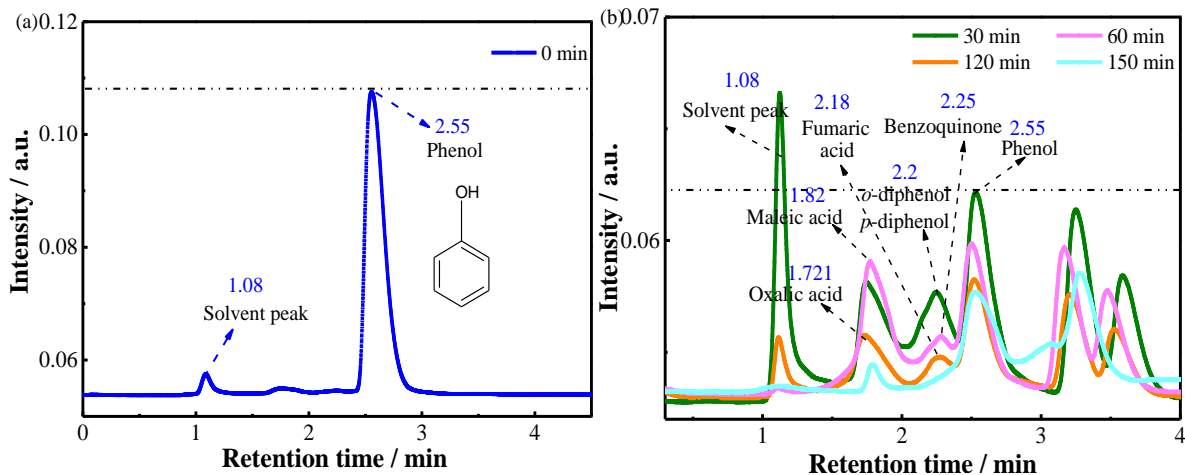


Figure S4. HPLC chromatograms of phenol degradation at different times (a), and proposed degradation mechanism of phenol by BMFe catalyst (b)

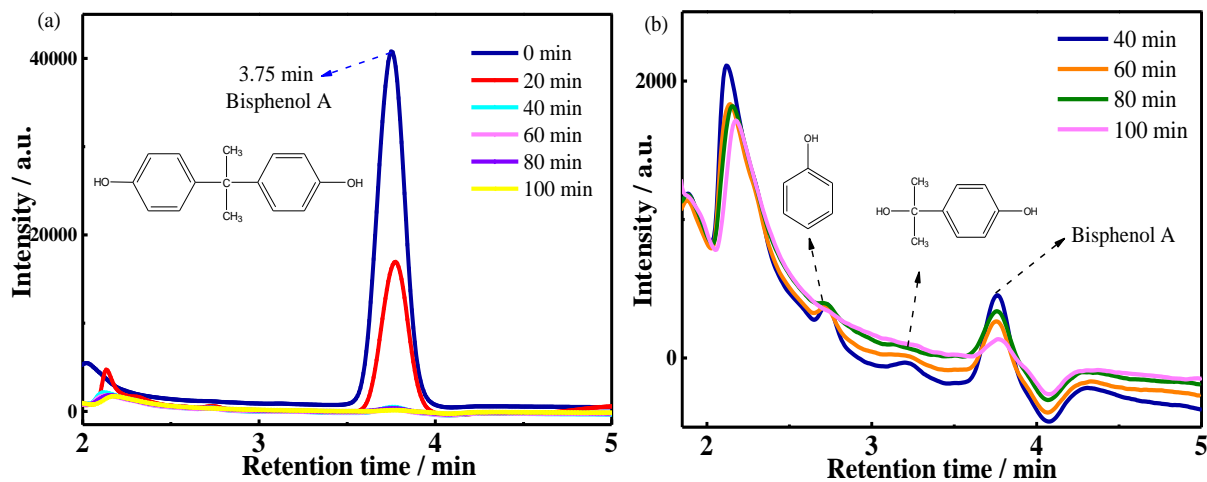


Figure S5. HPLC chromatograms of bisphenol A degradation via BMFe composite at different times (a) 0-100 min; (b) 40-100 min

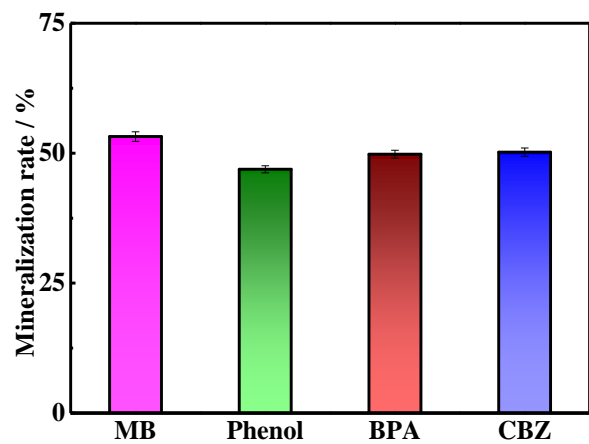


Figure S6. Mineralization rate of organic pollutants over BMFe-4 catalyst



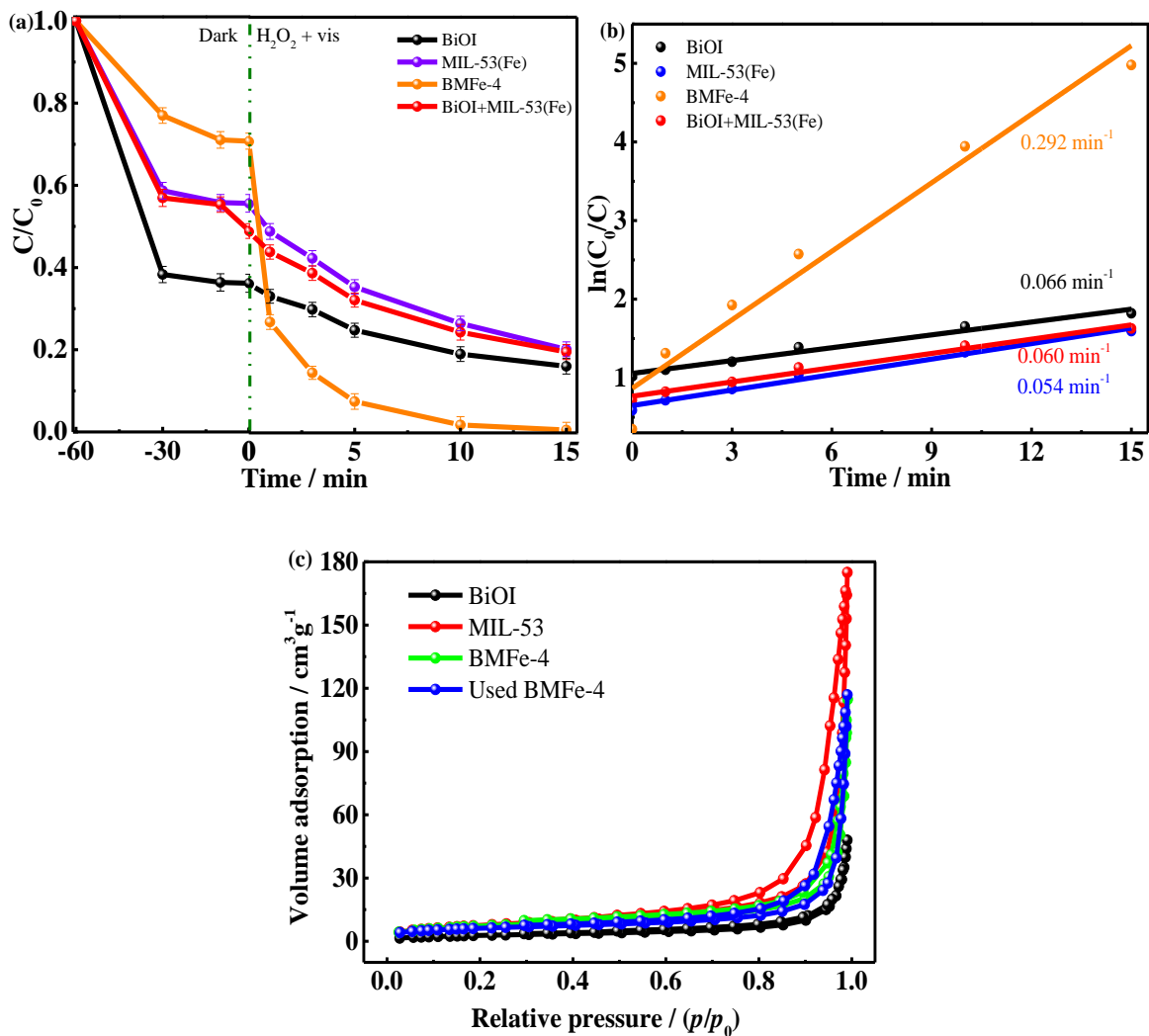


Figure S7. (a) Catalytic degradation of MB by individual BiOI, MIL-53(Fe), physically mixed B+MFe and BMFe-4; (b) Pseudo-first-order kinetics of degradation MB by individual BiOI, MIL-53(Fe), physically mixed B+MFe and BMFe-4; (c)  $N_2$  adsorption-desorption curves

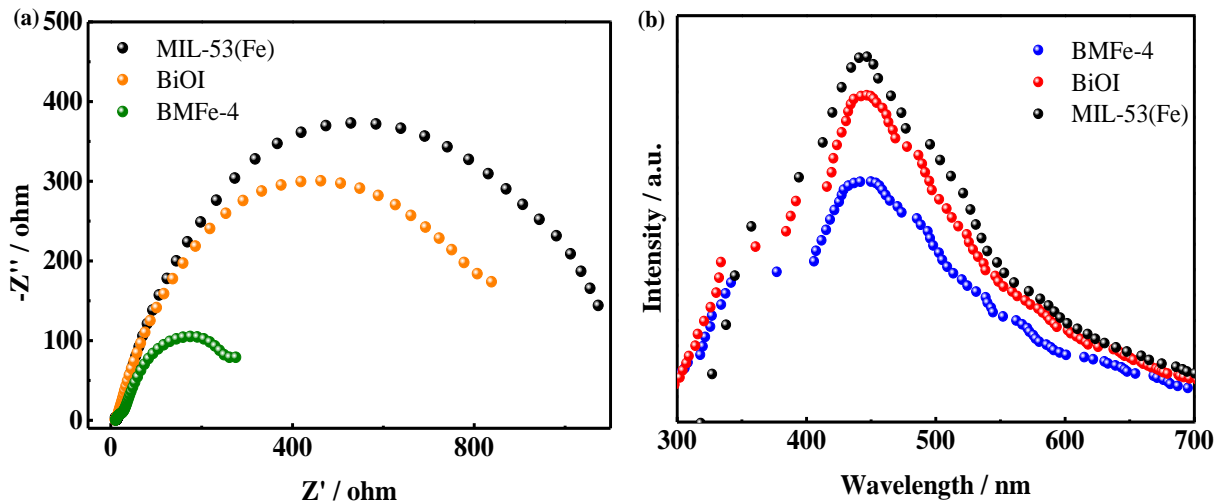


Figure S8. (a) EIS Nyquist plot and (b) PL spectra of BiOI, MIL-53(Fe) and BMFe-4 catalysts

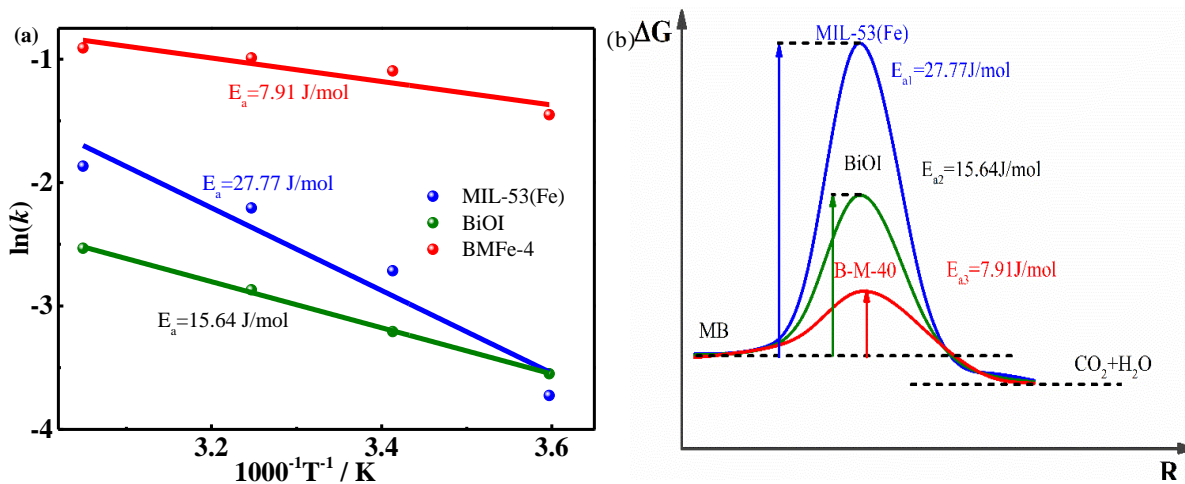


Figure S9. (a) Arrhenius plots of MB degradation rate  $\ln(k)$  vs  $1/T$ , (b) the apparent activation energy of the degradation of MB over MIL-53(Fe), BiOI and BMFe-4

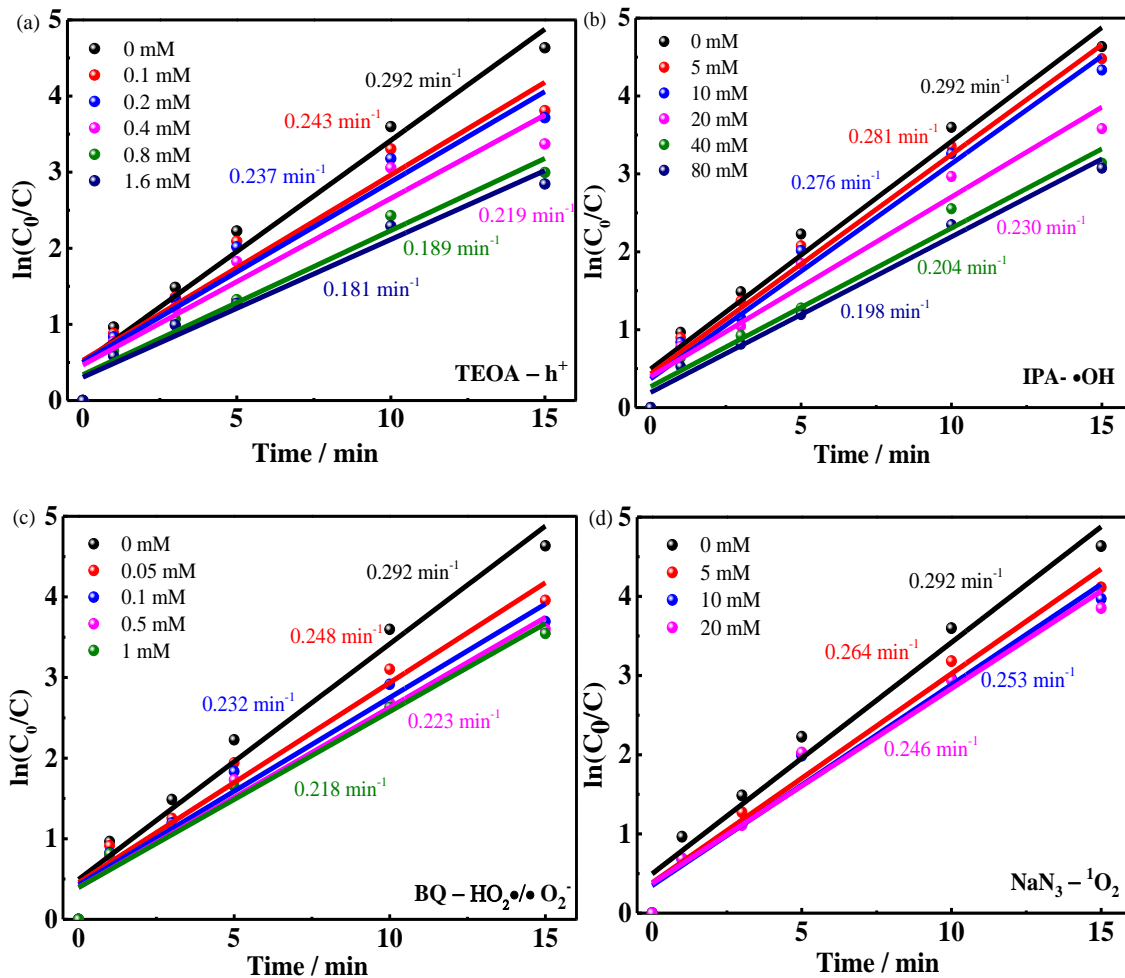


Figure S10. Effect of reactive species on the removal of MB in the B $\text{MFe-4}/\text{H}_2\text{O}_2/h\nu$  photo-Fenton system (a)  $h^+$ , (b)  $\bullet\text{OH}$ , (c)  $\bullet\text{O}_2^-/\text{HO}_2\bullet$  and (d)  ${}^1\text{O}_2$

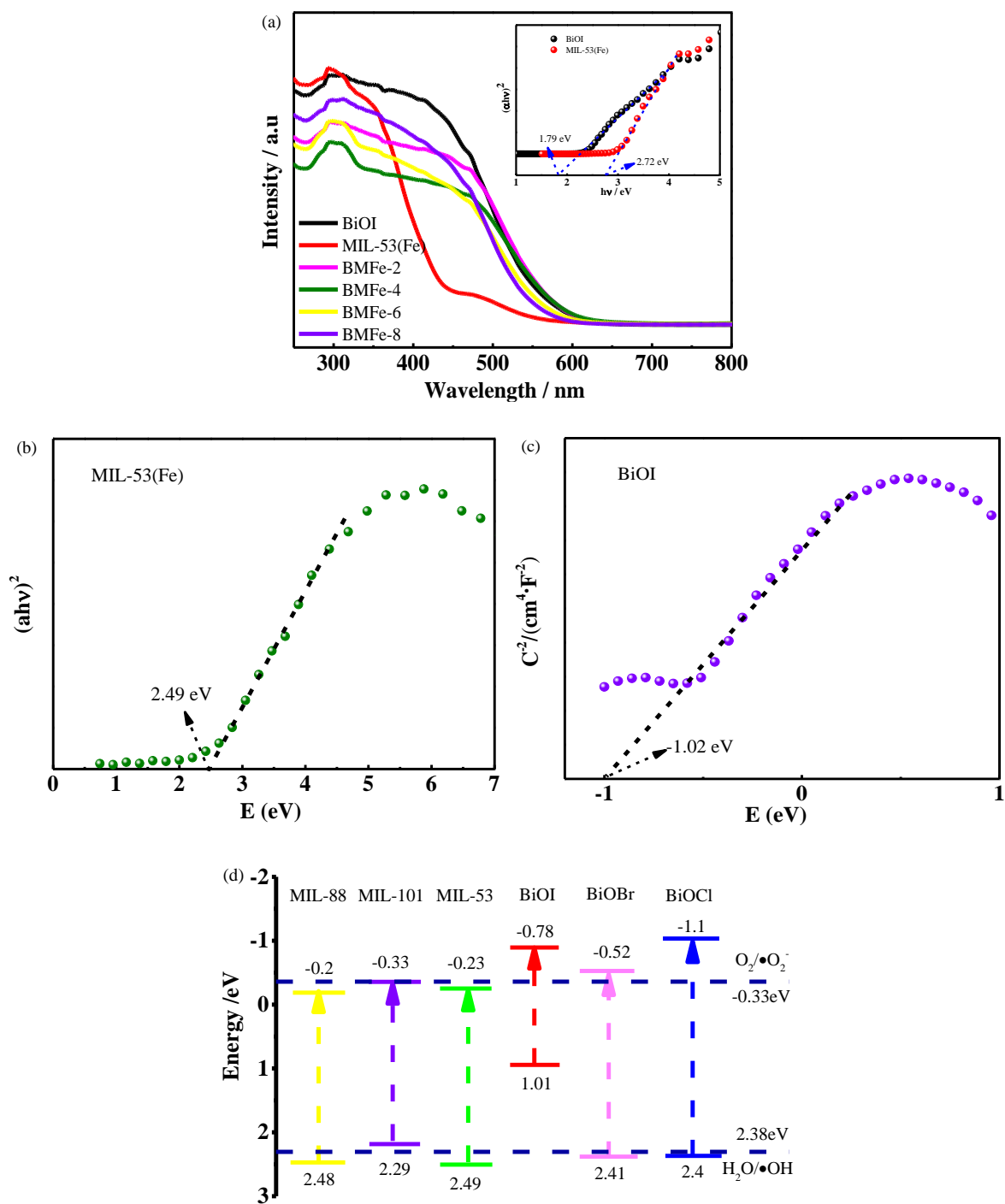


Figure S11. UV-vis DRS and plots of the  $(ah\nu)^2$  vs photo energy ( $h\nu$ ) (a), Band spectra of MIL-53(Fe) (b) and BiOI (c), band structure of Fe-MOFs and BiOX(Cl, Br, I) (d)

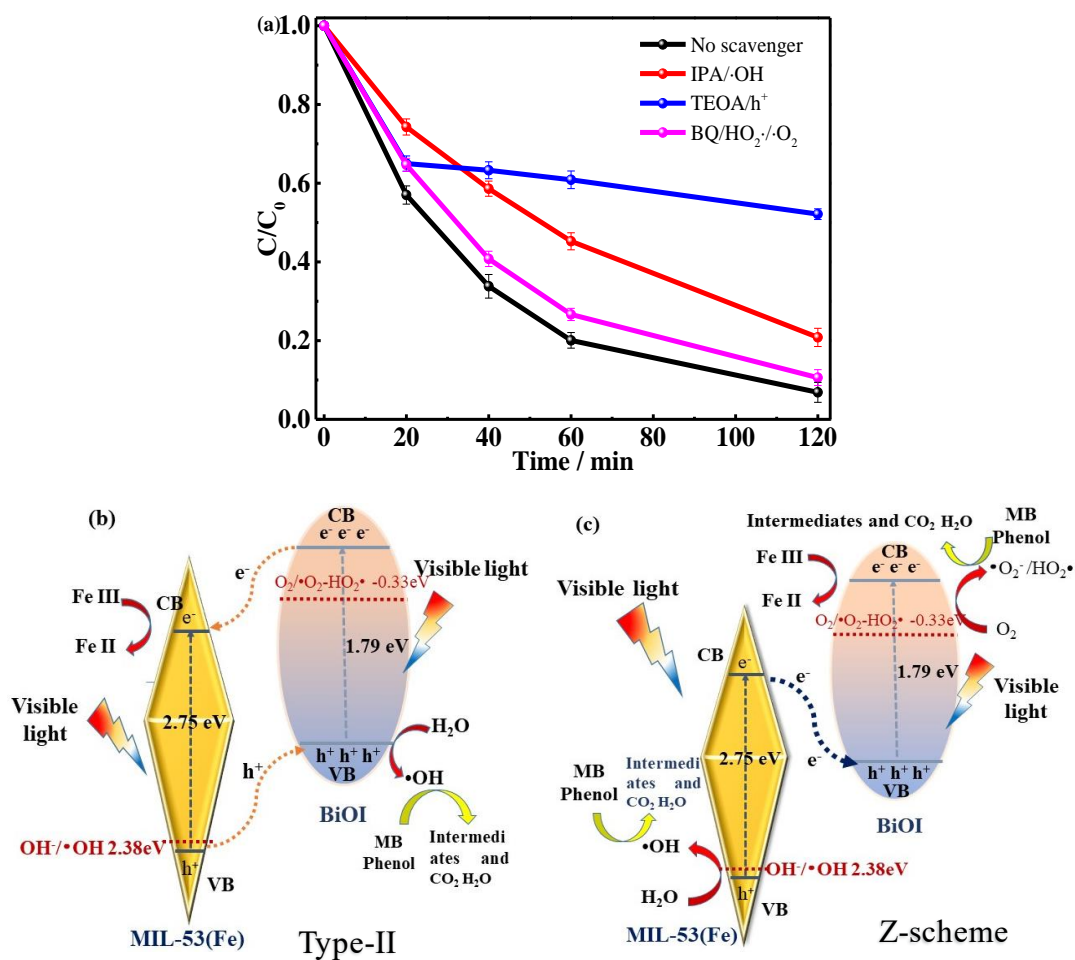


Figure S12. (a) Effect of different scavengers under photocatalytic system, (b) (c) Proposed charge transfer pathways of BMFe heterojunction

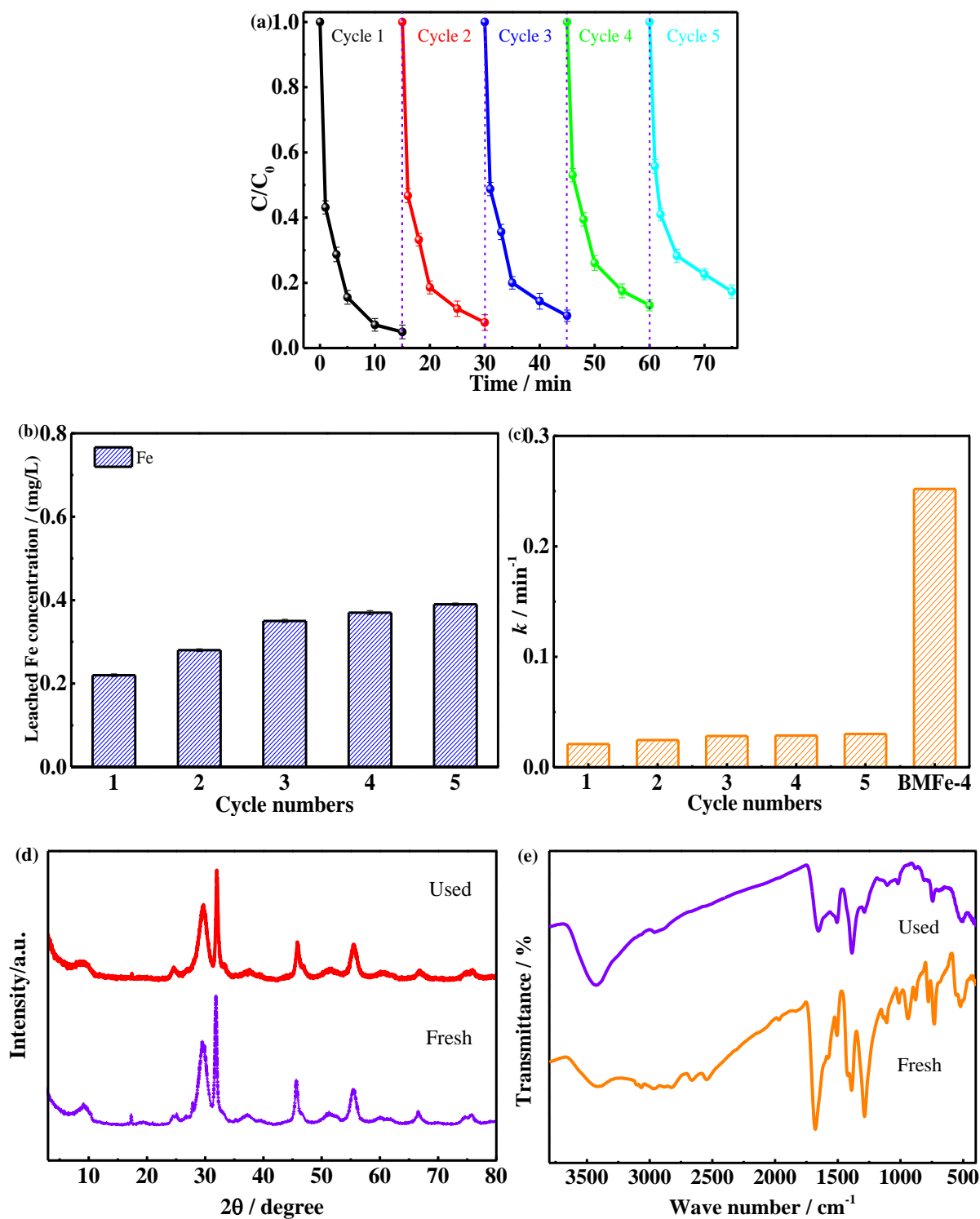


Figure S13. (a) Stability test for BMFe-4 catalyst photo-Fenton degradation MB; (b) The leached total iron concentration after each cycle, (c) the rate constants of the leached Fe iron compared with that of BMFe-4

(d) XRD pattern and (e) FTIR spectrum before and after five cycles

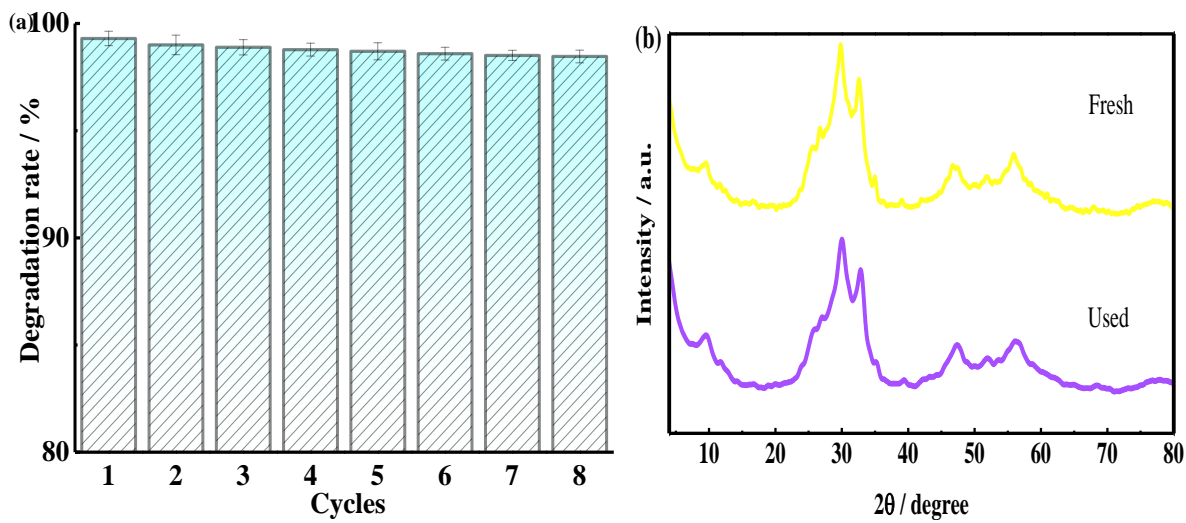
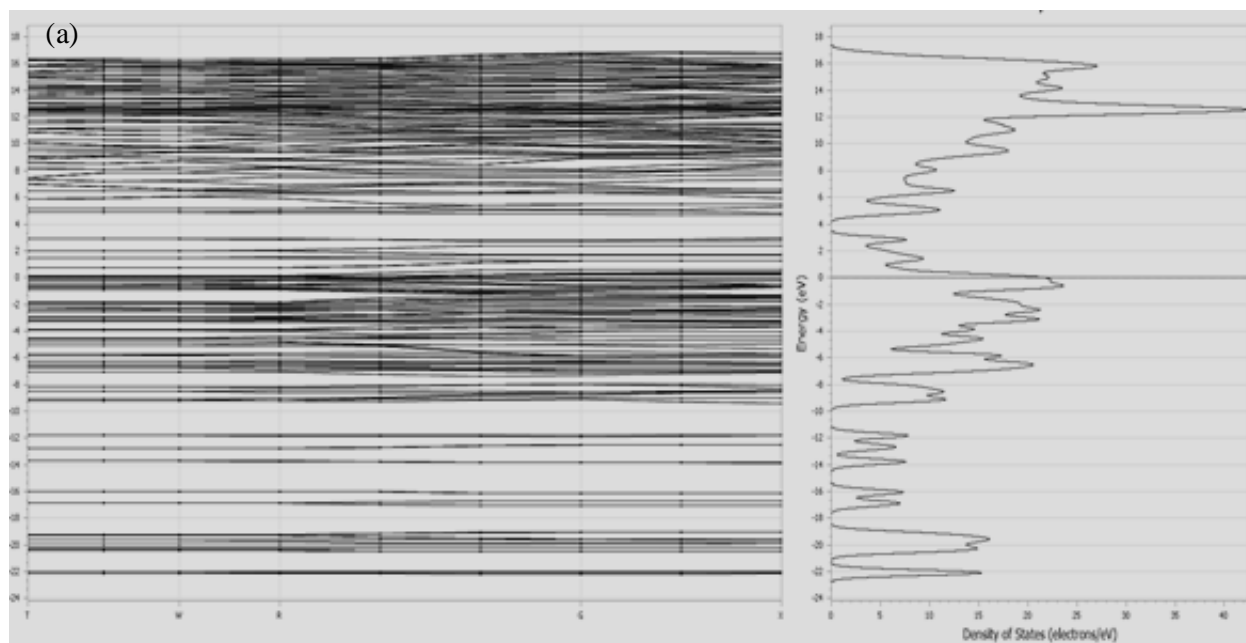


Figure S14. (a) Stability test of MB over BMFe-beads and (b) XRD pattern before and after cycles



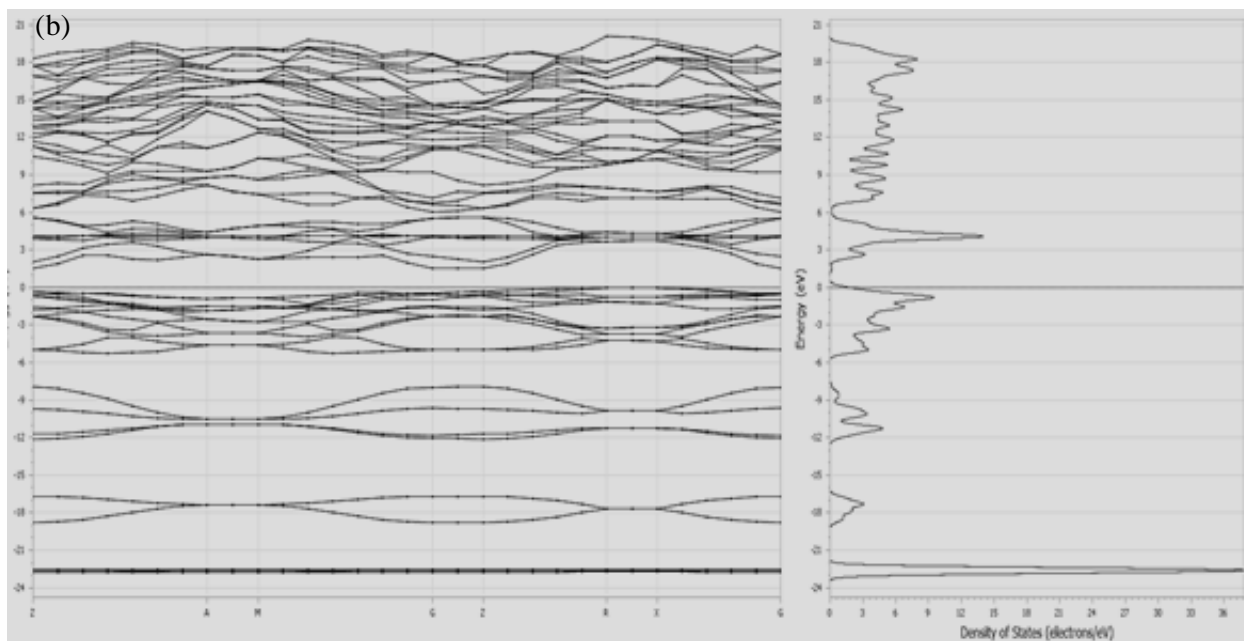


Figure S15. Band-structure and density of states of BiOI (a) and MIL-53(Fe) (b)

For in-depth understanding of the atomic and electronic structures, DFT modeling was conducted by comparing two different interface models: Interface of pristine BiOI, pristine MIL-53(Fe) and after optimization. The atomic structures of BiOI (110) surface and MIL-53(Fe) are displayed as the top and side-views in Figure 8a. Electronic DOS and Charge of difference show the mechanism of Z-scheme occurring at the interface.<sup>19</sup> Interfaces of stoichiometric structures and BMFe do not induce any in-gap state at the interface (Figure S15 and Figure 4); thus, photoexcited charge carriers are transferred along the band edges.<sup>20</sup>



## Reference

- (1) Zhang, M.; Lu, M.; Lang, Z. L.; Liu, J.; Liu, M.; Chang, J. N.; Li, L. Y.; Shang, L. J.; Wang, M.; Li, S. L.; Lan, Y. Q., Semiconductor/Covalent-Organic-Framework Z-Scheme Heterojunctions for Artificial Photosynthesis. *Angew Chem Int Ed Engl.* **2020**, *59*, 6500-6506.
- (2) Li, H.; Shan, C.; Pan, B., Fe(III)-Doped g-C<sub>3</sub>N<sub>4</sub> Mediated Peroxymonosulfate Activation for Selective Degradation of Phenolic Compounds via High-Valent Iron-Oxo Species. *Environmental Science & Technology.* **2018**, *52*, 2197-2205.
- (3) Zheng, S.; Chen, H.; Tong, X.; Wang, Z.; Crittenden, J. C.; Huang, M., Integration of a Photo-Fenton Reaction and a Membrane Filtration using CS/PAN@FeOOH/g-C<sub>3</sub>N<sub>4</sub> Electrospun Nanofibers: Synthesis, Characterization, Self-cleaning Performance and Mechanism. *Applied Catalysis B: Environmental.* **2021**, *281*, 119519.
- (4) Wang, W.; Zhao, W.; Zhang, H.; Dou, X.; Shi, H., 2D/2D Step-Scheme  $\alpha$ -Fe<sub>2</sub>O<sub>3</sub>/Bi<sub>2</sub>WO<sub>6</sub> Photocatalyst with Efficient Charge Transfer for Enhanced Photo-Fenton Catalytic Activity. *Chinese Journal of Catalysis.* **2021**, *42*, 97-106.
- (5) Wang, X.; Feng, J.; Zhang, Z.; Zeng, W.; Gao, M.; Lv, Y.; Wei, T.; Ren, Y.; Fan, Z., Pt Enhanced the Photo-Fenton Activity of ZnFe<sub>2</sub>O<sub>4</sub>/ $\alpha$ -Fe<sub>2</sub>O<sub>3</sub> Heterostructure Synthesized via One-Step Hydrothermal Method. *Journal of Colloid and Interface Science.* **2020**, *561*, 793-800.
- (6) Liao, X.; Wang, F.; Wang, Y.; Wei, W.; Xiao, Z.; Liu, H.; Hao, Q.; Lu, S.; Li, Z., Functionalized g-C<sub>3</sub>N<sub>4</sub> Sheets Assisted Synthesis of Growth-Oriented MIL-88B-Fe with Rod-Like Structure: Upgrading Framework Photo-Catalytic Performance and Stability. *Applied Surface Science.* **2020**, *503*, 144089.
- (7) Ahmad, M.; Quan, X.; Chen, S.; Yu, H., Tuning Lewis Acidity of MIL-88B-Fe with Mix-Valence Coordinatively Unsaturated Iron Centers on Ultrathin Ti<sub>3</sub>C<sub>2</sub> Nanosheets for Efficient Photo-Fenton Reaction. *Applied Catalysis B: Environmental.* **2020**, *264*, 118534.
- (8) Ahmad, M.; Chen, S.; Ye, F.; Quan, X.; Afzal, S.; Yu, H.; Zhao, X., Efficient Photo-Fenton Activity in Mesoporous MIL-100(Fe) Decorated with ZnO Nanosphere for Pollutants Degradation. *Applied Catalysis B: Environmental.* **2019**, *245*, 428-438.
- (9) Guo, B.; Xu, T.; Zhang, L.; Li, S., A Heterogeneous Fenton-like System with Green Iron Nanoparticles for the Removal of Bisphenol A: Performance, Kinetics and Transformation Mechanism. *Journal of Environmental Management.* **2020**, *272*, 111047.
- (10) Fu, H.; Song, X.-X.; Wu, L.; Zhao, C.; Wang, P.; Wang, C.-C., Room-Temperature Preparation of MIL-88A as a Heterogeneous Photo-Fenton Catalyst for Degradation of Rhodamine B and Bisphenol A under Visible Light. *Materials Research Bulletin.* **2020**, *125*, 110806.
- (11) Sun, S.; Yao, H.; Fu, W.; Liu, F.; Wang, X.; Zhang, W., Enhanced Degradation of Carbamazepine in FeOCl based Photo-Fenton Reaction. *Journal of Environmental Chemical Engineering.* **2020**, *9*, 104501.
- (12) Gao, Y.; Yu, G.; Liu, K.; Deng, S.; Wang, B.; Huang, J.; Wang, Y., Integrated Adsorption and Visible-Light Photodegradation of Aqueous Clofibrac Acid and Carbamazepine by a Fe-based Metal-Organic Framework. *Chemical Engineering Journal.* **2017**, *330*, 157-165.
- (13) Cao, J.; Li, X.; Lin, H.; Chen, S.; Fu, X., In Situ Preparation of Novel p-n Junction Photocatalyst BiOI/(BiO)<sub>2</sub>CO<sub>3</sub> with Enhanced Visible Light Photocatalytic Activity. *J Hazard Mater.* **2012**, *239-240*, 316-24.
- (14) Hu, H.; Zhang, H.; Chen, Y.; Chen, Y.; Zhuang, L.; Ou, H., Enhanced Photocatalysis Degradation of Organophosphorus Flame Retardant using MIL-101(Fe)/Persulfate: Effect of Irradiation Wavelength and Real Water Matrixes. *Chemical Engineering Journal.* **2019**, *368*, 273-284.
- (15) Chaturvedi, G.; Kaur, A.; Kansal, S. K., CdS-Decorated MIL-53(Fe) Microrods with Enhanced Visible Light Photocatalytic Performance for the Degradation of Ketorolac Tromethamine and Mechanism Insight. *The Journal of Physical Chemistry C.* **2019**, *123*, 16857-16867.
- (16) Cui, D.; Wang, L.; Du, Y.; Hao, W.; Chen, J., Photocatalytic Reduction on Bismuth-Based p-Block Semiconductors. *ACS Sustainable Chemistry & Engineering.* **2018**, *6*, 15936-15953.

- (17) Han, Q.; Dong, Y.; Xu, C.; Hu, Q.; Dong, C.; Liang, X.; Ding, Y., Immobilization of Metal-Organic Framework MIL-100(Fe) on the Surface of BiVO<sub>4</sub>: A New Platform for Enhanced Visible-Light-Driven Water Oxidation. *ACS Appl Mater Interfaces*. **2020**, *12*, 10410-10419.
- (18) Liu, R.; Xu, Y.; Chen, B., Self-Assembled Nano-FeO(OH)/Reduced Graphene Oxide Aerogel as a Reusable Catalyst for Photo-Fenton Degradation of Phenolic Organics. *Environ Sci Technol*. **2018**, *52*, 7043-7053.
- (19) Wong, K. T.; Kim, S. C.; Yun, K.; Choong, C. E.; Nah, I. W.; Jeon, B.-H.; Yoon, Y.; Jang, M., Understanding the Potential Band Position and e<sup>-</sup>/h<sup>+</sup> Separation Lifetime for Z-Scheme and Type-II Heterojunction Mechanisms for Effective Micropollutant Mineralization: Comparative Experimental and DFT Studies. *Applied Catalysis B: Environmental*. **2020**, *273*, 119034.
- (20) Wang, Y.; Zhu, C.; Zuo, G.; Guo, Y.; Xiao, W.; Dai, Y.; Kong, J.; Xu, X.; Zhou, Y.; Xie, A.; Sun, C.; Xian, Q., 0D/2D Co<sub>3</sub>O<sub>4</sub>/TiO<sub>2</sub> Z-Scheme Heterojunction for Boosted Photocatalytic Degradation and Mechanism Investigation. *Applied Catalysis B: Environmental*. **2020**, *278*, 119298.